NUMERICAL INVESTIGATION THE FLOW DISTRIBUTION CHARACTERISTICS OF THE EVAPORATIVE COOLING PLATE IN A PUMP-DRIVEN TWO-PHASE FLOW SYSTEM

Nianyong ZHOU[1*], Wenyu LV[1], Yang LIU[2], Guanghua TANG[1], Qingguo BAO[1], Youxin ZOU[1], Yingjie ZHAO[1]

1 School of Petroleum Engineering, Changzhou University, Changzhou, 213164, Jiangsu, China

2 Avic Xinxiang Aviation industry (Group) Co., LTD, Xinxiang,453049, Henan, China

[*]Corresponding Authors: zhounianyong@cczu.edu.cn

The uniformity of flow distribution within the evaporative cooling plate is essential for its heat transfer performance, given its role as the core component in the pump-driven two-phase flow cooling system. Nevertheless, traditional technical methods employed to achieve uniform flow distribution, such as using an external head and an internal large-diameter sump, lead to a cold plate with excessive volume and weight, rendering it unsuitable for numerous engineering applications. In response to these challenges, this paper introduces a novel flow distribution structure that integrates a spoiler column with a sump. Numerical simulation is utilized to examine the flow distribution characteristics of this structure. The study examines the influence of factors, including the inlet and outlet positions, sump width, and spoiler column distribution, on the flow distribution characteristics. The findings suggest that, for micro-channel cold plates, achieving a more uniform flow distribution is possible by positioning the inlet and outlet closer to the center of the sump. An increase in the sump width proves effective in reducing the non-uniformity of the flow distribution. Furthermore, the addition of a spoiler column at both the inlet and outlet positions results in a significant reduction in non-uniformity. Alternatively, adding a spoiler column at the inlet alone can also yield positive results. Overall, among the eight working conditions analyzed in this paper, the cold plate exhibits a maximum reduction of 80% in overall flow distribution non-uniformity.

Keywords*: Pump-driven Two-phase Flow System, Evaporation Cooling Plate, Flow Distribution, Numerical Simulation*

1. Introduction

As electronic equipment progressively miniaturizes and integrates at higher levels, the challenges associated with heat dissipation and temperature control become increasingly pronounced. The conventional heat dissipation method is inadequate for fulfilling cooling demands characterized by high precision and substantial heat flux. In response to these challenges, there has been considerable interest in pump-driven two-phase flow cooling technology, attributed to its advantages encompassing excellent heat transfer performance, low flow resistance, and high-temperature uniformity. Numerous scholars [1-4] have conducted extensive research in areas including filling capacity, heat load, and undercooling. In these investigations, the evaporative cooling plate serves as the pivotal component of the pump-driven two-phase flow system, directly influencing the overall performance of the cooling system. Nevertheless, the heat transfer performance of the evaporative cooling plate is influenced by various factors, including channel shape, evaporation temperature, working medium flow, flow distribution, gap leakage, etc. However, among these factors, the in-depth exploration of flow distribution requires further attention [5, 6].

Presently, numerous scholars are predominantly concentrating their research efforts on optimizing the inlet or head structure when studying the flow distribution characteristics of evaporative cooling plates. When studying the pump-driven two-phase flow cooling system, Setyawan et al. [7] and Jiang [8] used a flat evaporative cooling plate in their test device and ensured uniform flow distribution of the cooling plate by using the external liquid collecting pipe and the internal liquid collecting chamber structures, which accounted for about 40% of the total volume of the evaporator. Wang et al. [9] implemented a head diversion structure at both ends to achieve uniform flow distribution in the evaporator, resulting in a approximately 40% increase in the evaporator's volume. In the absence of specific research data on pump-driven two-phase flow cooling plates, findings from studies on micro-channel evaporators can serve as a valuable reference. Wu et al. [10] conducted experimental research on six types of deflector structures and observed that the gas and liquid distribution in the tri-symmetric deflector structure was superior, however, it resulted in an approximately 18% increase in the evaporator's volume. Peng et al. [11] incorporated a deflector into the evaporator head structure and assessed its impact on the uniformity of liquid separation through computational fluid dynamics (CFD) analysis. The enhanced deflector led to a 91.5% reduction in flow distribution unevenness in the inlet header but resulted in a 42% increase in the evaporator's volume. Byun et al. [12] conducted experimental research on the impact of a horizontally inserted shunt plate in the inlet shunt tube on the uniformity of fluid distribution in the heat exchanger. Their findings suggest that the insertion of a perforated round tube into the inlet collecting tube effectively enhances fluid distribution in the heat exchanger. Additionally, the design of the collecting tube results in an approximately 33% increase in the evaporator's volume. Yuan et al. [13] employed numerical simulation methods to investigate the uniformity of refrigerant distribution in a parallel flow heat exchanger, considering both configurations with and without a splitter plate. Their findings revealed that incorporating a splitter plate in the head enhances flow distribution uniformity but concurrently results in an approximately 35% increase in the evaporator's volume. Wei et al. [14] introduced a novel head structure for the parallel flow heat exchanger. They conducted simulations and analyses to assess the impact of two distinct inlet modes on the flow distribution in each channel within the new structure. However, the introduction of this new structure resulted in an approximately 42% increase in the evaporator's volume. Gao et al. [15] devised two variable-aperture splitter plate structures and concluded that the new splitter plate can notably enhance the overall flow distribution uniformity of the fluid. However, this improvement is accompanied by an approximately 31% increase in the evaporator's volume. Tian et al. [16] proposed optimizing the structure of micro-channels by introducing a widened microchannel structure with transverse microcavities. This modification resulted in a 37.5% improvement in overall flow uniformity, but it increased the evaporator's volume by about 35%. Redo et al. [17] designed a vertical dual-chamber head structure that demonstrates improved flow distribution under low mass flow conditions compared to traditional heads. However, this design resulted in an approximately 21% increase in the evaporator's volume. Siddique et al. [18] designed a novel dumbbell-shaped collector with the aim of achieving uniform flow distribution in parallel microchannel evaporators, and they quantitatively evaluated its performance. They observed that its performance surpassed that of all existing shapes, however, it resulted in an approximately 43% increase in the evaporator's volume. Meanwhile, Wu et al. [19] introduced a novel embedded baffle distributor for a micro-channel heat exchanger. This distributor demonstrated more than 40% lower non-uniformity in vertical, inclined, and horizontal installations when compared to the traditional cylindrical distributor. Nevertheless, the distributor structures constituted approximately 50% of the total evaporator's volume. Ye et al. [20] examined the influence of two liquid separation structures—the addition of a liquid separation tube and an orifice plate—on flow distribution in a cold plate using numerical simulation. The results indicated that the uniformity of the mixed phase in the optimal liquid separation tube scheme and the optimal orifice plate scheme was 56% and 60.80% higher than that of the baseline, respectively. However, the incorporation of these two structures led to a 26% and 30% increase in the evaporator's volume, respectively.

While prior studies have notably enhanced the uniformity of flow distribution in the evaporator, they overlooked the consideration of the evaporator's volume, potentially restricting its practical applications. This paper tackles this issue through an exploration of a built-in sump structure, effectively minimizing the volume of the cold plate. The investigation delves into the influence of structural parameters—including the inlet and outlet, the sump, and the spoiler column—on the flow distribution characteristics of the pump-driven two-phase flow cold plate. The objective is to pinpoint the optimal structure that ensures uniform flow distribution.

2. Physical model

2.1 3D model

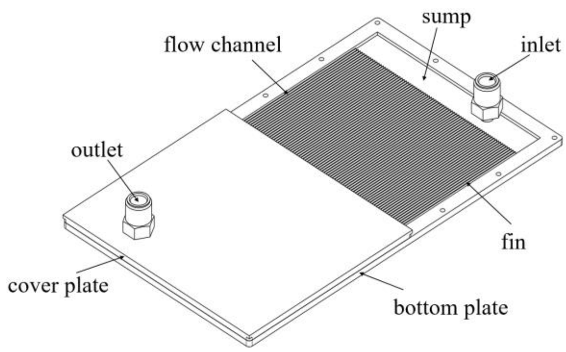

Fig. 1 Three-dimensional model of evaporation cooling plate of the pump-driven two-phase flow system

The physical model explored in this paper is an evaporative cooling plate within a pump-driven two-phase flow system, comprising a cover plate and a bottom plate. As illustrated in **Figure 1**, the structure takes the form of a plate, with dimensions of 250mm in length, 160mm in width, and 6mm in height. The cold plate consists of individual flow channels, each with a length of 210mm, a width of 1.4mm, and a height of 2mm. The spacing between adjacent channels is 1.8mm, and there are 78 channels arranged horizontally and in parallel. The inlet and outlet positions of the cold plate are situated on the cover plate, positioned 2mm above the sump. The cold plate employs an internal sump structure. In contrast to an external sump, this design reduces the cold plate volume by approximately 25%, resulting in significant savings in assembly space.

2.2 Mathematical model

2.2.1 Control equation

To facilitate modeling and solving, the following assumptions are made: 1) The working fluid is an ideal and incompressible fluid. 2) Pressure changes' influence on physical properties is neglected. 3) Inlet velocity and temperature distributions are assumed to be uniform. Additionally, studies have demonstrated that the Eulerian model effectively replicates the gas-liquid separation phenomenon in two-phase flow based on experimental results [21, 22]. Therefore, this study employs the Eulerian model as the two-phase flow model. Given the highly turbulent nature of the refrigerant flow inside the evaporative cold plate, the standard k-ε model is utilized to ensure precision in turbulence calculations.

(1) Continuity Equation：

$$\frac{\partial \alpha_l}{\partial t} + \nabla \cdot (\boldsymbol{v}\alpha_l) = \frac{\boldsymbol{S}}{\rho_l} \#(1)$$

$$\frac{\partial \alpha_g}{\partial t} + \nabla \cdot \left(\boldsymbol{v}\alpha_g\right) = \frac{\boldsymbol{S}}{\rho_g} \#(2)$$

where α_l and α_g is the volume fraction of the liquid and gas phases, $\alpha_l + \alpha_g = 1$, $\boldsymbol{v}$ is the velocity vector, $\boldsymbol{S}$ is the quality source term, T is the time.

(2) Momentum Equation：

$$\frac{\partial(\rho\boldsymbol{v})}{\partial t} + \nabla \cdot (\rho\boldsymbol{v}\boldsymbol{v}) = -\nabla p + \nabla \cdot \left[\mu(\nabla v + \nabla v^T) - \frac{2}{3}\mu\nabla \cdot \boldsymbol{v}\boldsymbol{I}\right] + \rho\boldsymbol{a}_h + \boldsymbol{F}_{vol} \#(3)$$

where $\boldsymbol{I}$ is the unit tensor, $\boldsymbol{a}_h$ is the overload vector, $\boldsymbol{F}_{vol}$ is the volumetric force.

(3) Energy Equation：

$$\frac{\partial(\rho E)}{\partial t} + \nabla \cdot [\boldsymbol{v}(\rho E + p)] = \nabla \cdot (\lambda\nabla T) + Q \#(4)$$

where E is energy, λ is the thermal conductivity coefficient; Q is the energy source term.

The physical properties of the gas-liquid mixture and energy in the control equation can be calculated by averaging the volume fraction.

$$\rho = \alpha_l\rho_l + \alpha_g\rho_g \#(5)$$

$$\mu = \mu_l\rho_l + \mu_g\rho_g \#(6)$$

$$\lambda = \alpha_l\lambda_l + \alpha_g\lambda_g \#(7)$$

$$E = \frac{\alpha_l\rho_l E_l + \alpha_g\rho_g E_g}{\alpha_l\rho_l + \alpha_g\rho_g} \#(8)$$

$$E_l = c_{p,l}(T_l - T_{sat}) \#(9)$$

$$E_g = c_{p,g}\left(T_g - T_{sat}\right) \#(10)$$

The surface tension between gas-liquid phases can be calculated using the continuous surface force model proposed by Brackbill et al. [23] This model considers surface tension as a volumetric force acting on the fluid within the mesh elements of the phase interface region and introduces it into the momentum equation.

$$F_v = \sigma\frac{\alpha_l\rho_l\kappa_g\nabla\alpha_g + \alpha_g\rho_g\kappa_l\nabla\alpha_l}{\frac{1}{2}\left(\rho_l + \rho_g\right)} \#(11)$$

where κ is the surface curvature, and σ is the surface tension.

The mass source term $\boldsymbol{S}$ generated by flow boiling can be calculated using the Lee [24] model, while the energy source term Q is the product of the mass source term and the latent heat of vaporization.

$$\boldsymbol{S} = \begin{cases} r_l \alpha_l \rho_l \dfrac{T_l - T_{sat}}{T_{sat}}, & T_l \geq T_{sat} \\ r_g \alpha_g \rho_g \dfrac{T_{sat} - T_g}{T_{sat}}, & T_g < T_{sat} \end{cases} \#(12)$$

$$Q = -\boldsymbol{S} h_{lg} \#(13)$$

where r_l and r_g are the evaporation frequency and condensation frequency, which can be understood as a time relaxation coefficient, h_{lg} is the latent heat of gasification.

2.2.2 boundary conditions

The inlet boundary condition is defined as a velocity inlet, with the cooling refrigerant R134a entering at the initial temperature of T_{in} and a flow rate of V_{in}. The bottom heating wall is subjected to constant heat flux density q_w, and the undefined wall is treated as an adiabatic wall. The outlet boundary condition is set as a pressure outlet. For the near-wall region, the standard wall function method is employed, and velocity and pressure are coupled using the SIMPLEC method. A second-order upwind scheme is used to solve all discrete equations. The specific values for calculating the working conditions are presented in **Table 1.**

Table 1. Calculation Conditions

Initial conditions	Inlet temperature T_{in}	Inlet flow velocity V_{in}	Inlet and outlet turbulence intensity	Heat flux density q_w
Specific values	291.15K	0.35m/s	5%	100W/cm^2

2.3 Flow characteristics analysis of simplified model

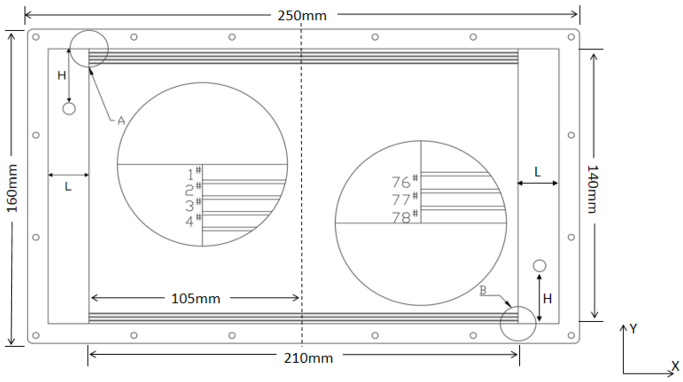

Fig. 2 Simplified model of the evaporative cooling plate

For ease of calculation, the structure was partially simplified. The channels in the cold plate are numbered 1#~78# from top to bottom, where H represents the distance between the inlet and outlet positions and the side wall of the cold plate, and L represents the width of the sump. And to better observe the velocity of each channel, a dashed line profile was set on the cold plate in the XY axis direction. The simplified model is depicted in **Figure 2**.

Eight types of pump-driven two-phase flow cooling plates with different structures were designed in this study, as shown in **Table 2**, including modifications to the inlet and outlet positions (A-C type), the sump's structure (C-E type), and the spoiler column (F-H type) at the inlet and outlet. The length and width of the flow channel remain unchanged for all eight cooling plate structures.

Table 2. Model parameters of eight different structures

Model No	Width of sump L(mm)	Distance between inlet and outlet position and upper wall H(mm)	Whether there is a spoiler column at the inlet	Whether there is a spoiler column at the outlet
A	20	5	no	no
B	20	40	no	no
C	20	80	no	no
D	15	80	no	no
E	10	80	no	no
F	20	80	yes	no
G	20	80	no	yes
H	20	80	yes	yes

3. Grid independence verification

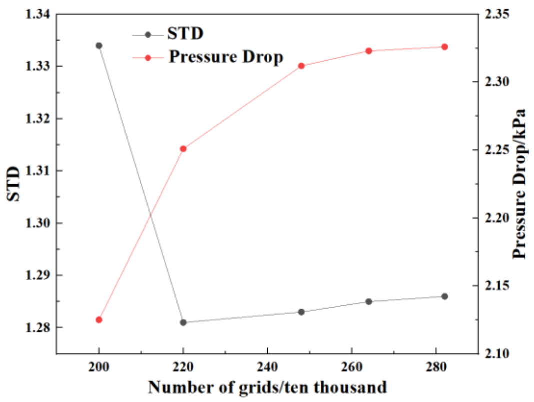

Fig. 3 Grid independence verification

Grid independence verification was performed to ensure accurate calculations. Ultimately, it was determined that the grid numbers for the three types of structures, involving different inlet and outlet positions, varied sump structural parameters, and the addition of a spoiler column, were 2.2 million, 2.48 million, and 2.64 million, respectively. At this stage, both the standard deviation (STD) of the mixed-phase flow rate and the change in pressure drop of the pump-driven two-phase flow cooling plate are less than 1%. As an example, for the evaporative cooling plate of the pump-driven two-phase flow system with a spoiler column at the inlet, the grid independence verification is depicted in **Figure 3**. The calculation utilized 2.64 million grids.

4. Verification of numerical simulation methods

To examine the numerical simulation methodology for a pump-driven two-phase flow evaporative cooling plate, we established an experimental platform for the pump-driven two-phase flow system. The physical images of the main components of the experimental system are illustrated in **Figure 4**. Subsequent experiments were carried out using the pump-driven two-phase flow test rig, with experimental parameters and conditions specified in **Table 3**.

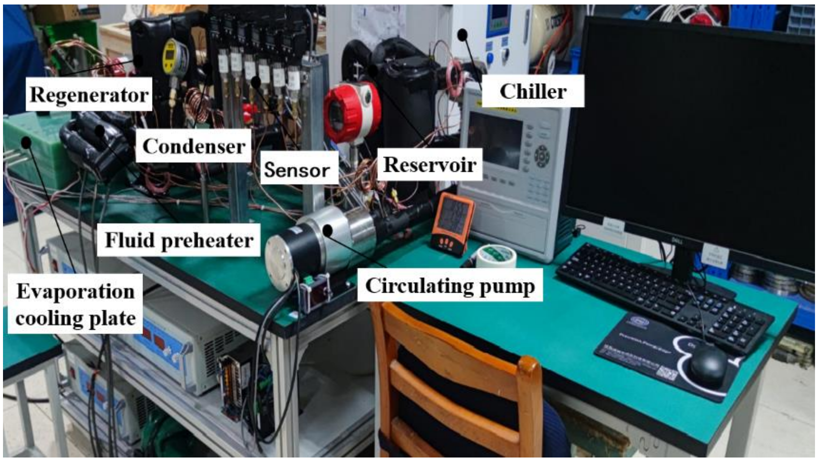

Fig. 4 Physical images of the main components and devices of the pump driven two-phase flow system

Table 3. Main Parameters of the Experimental System

Experiment parameter	Inlet temperature	Experimental voltage	Experimental current	Saturation pressure
	292.15K	159.9V	13.17A	0.5MPa

Table 4. Comparison of experimental and simulated values

	Heat transfer quantity(kW)	Heat transfer coefficient (W·m^{-2}·K^{-1})	Outlet temperature (K)	Refrigerant outlet vapor quality
Mass flow q_m=0.0405kg/s				
Experimental data	2.46	6605.12	293.29	0.331
Simulation data	2.81	6953.25	293.56	0.378
Error	12.46%	5.01%	0.09%	12.43%
Mass flow q_m=0.0512kg/s				
Experimental data	3.53	7924.38	293.97	0.375
Simulation data	3.35	7635.42	293.53	0.356
Error	5.10%	3.65%	0.15%	5.07%
Mass flow q_m=0.0613kg/s				
Experimental data	4.32	9124.93	294.08	0.384
Simulation data	3.84	8724.38	293.37	0.341
Error	11.11%	4.39%	0.24%	11.20%

When the heating power is constant, by varying the mass flow rate within the evaporative cooling plate, a comparison of experimental and simulated values for outlet dryness, outlet temperature, heat transfer quantity, and heat transfer coefficient was conducted. A comparison between the experimental measurements and simulated results was conducted, and the errors are presented in **Table 4**. The errors meet the requirements for engineering calculations, thereby validating the accuracy of the numerical simulation. Consequently, the investigated simulation method for the pump-driven two-phase flow evaporative cooling plate is deemed feasible.

5. Results and analysis

To investigate the non-uniformity of flow distribution in heat exchangers, the non-uniformity of channel flow distribution ε and total flow distribution S_t were employed as metrics [25]. The definition formula is:

$$\varepsilon = \frac{m_i - m_a}{m_a} \#(14)$$

$$S_t = \sqrt{\frac{1}{n-1}\sum_{i=1}^{n}\left(\frac{m_i}{m_a} - 1\right)^2} \#(15)$$

Where m_i is the fluid flow in the number i channel, m_a is the average fluid flow in a single channel, n is the total number of channels. The closer the values of total flow distribution unevenness S_t and flow distribution unevenness ε are to 0, the more uniform the flow distribution of the cold plate is.

5.1 Impact of inlet and outlet position on flow distribution uniformity

With the width of the cold plate sump held constant, the article simulates three different structures with H=5mm, 40mm, and 80mm to analyze the influence of inlet and outlet positions on the uniformity of flow distribution.

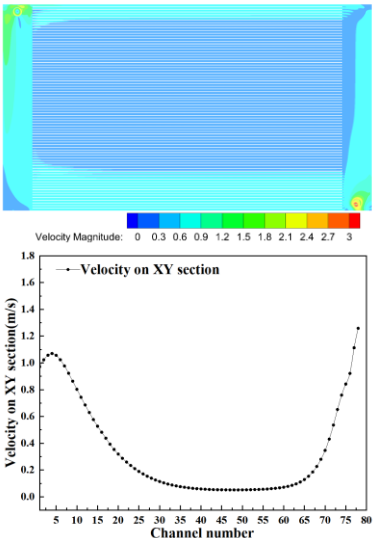

Fig. 5 Velocity contour of the cooling plate and velocity curve of each channel in the XY section when *H*=5mm

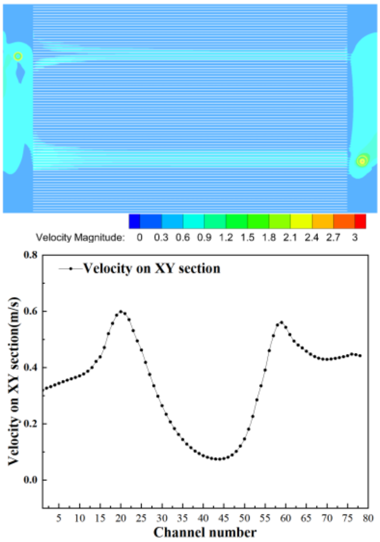

Fig. 6 Velocity contour of the cooling plate and velocity curve of each channel in the XY section when *H*=40mm

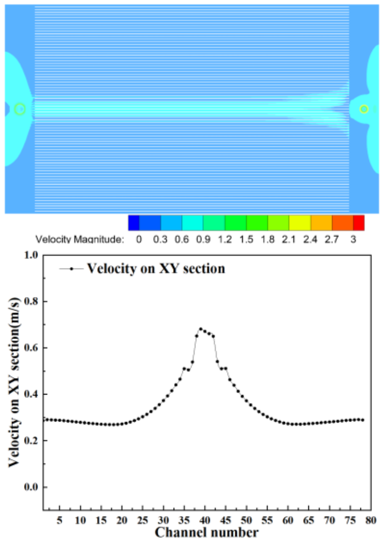

Fig. 7 Velocity contour of the cooling plate and velocity curve of each channel in the XY section when *H*=80mm

Figures 5-7 depict the velocity contour of the cold plate at different inlet and outlet positions, along with the velocity curve of each channel in the XY section (The cross-sectional position is at the dashed line in Figure 2). The figures reveal prominent peaks in the three velocity charts, indicating that channels closer to the inlet and outlet positions have higher velocities. Conversely, channels further away from the inlet and outlet exhibit lower flow velocities. **Figure 5** illustrates that channel 35 to 60 exhibit negligible fluid flow, while channels 1 to 10 and 73 to 78 experience high fluid velocities exceeding 0.75 m/s, with a maximum difference of approximately 1.10 m/s. This indicates severe unevenness in the flow distribution of the cold plate. The reason is that, as the fluid enters the cold plate from top to bottom, a large amount of it converges at the inlet position, forming vortices.

The existence of vortices in the sump is a crucial factor contributing to the uneven refrigerant flow distribution in the evaporative cold plate.

Figures 5 to 7 show that a smaller *H* value, specifically when the inlet and outlet positions are closer to the upper wall of the cold plate, leads to a flow distribution pattern with reduced flow in the middle and increased flow on both sides. Consequently, there is minimal flow in the central part of the channel. As the inlet and outlet positions move towards the middle, fluid flows through each channel, and when they reach the middle of the sump (*H*=80mm), the flow distribution pattern of each channel changes significantly, resulting in a relatively uniform flow distribution. Thus, the position of the inlet and outlet has a significant impact on the flow distribution uniformity of the evaporative cooling plate.

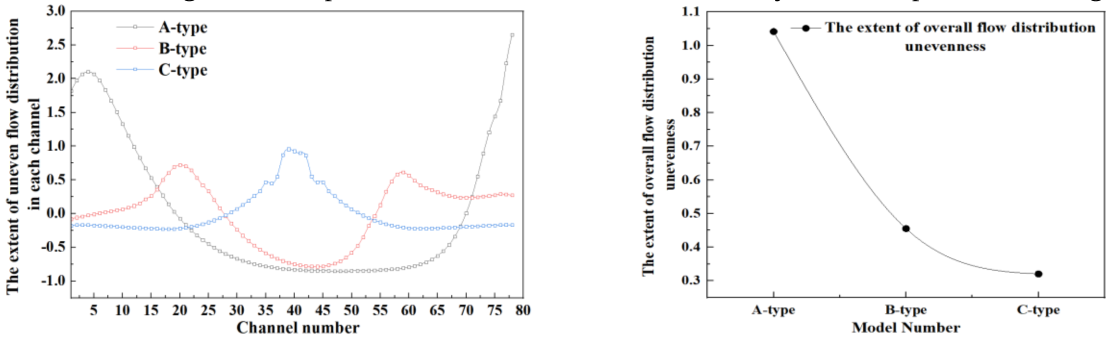

(a) The extent of uneven flow distribution in each channel **(b) The extent of overall flow distribution unevenness**

Fig. 8 Comparison of cold plates at three different inlet and outlet positions

Figure 8 illustrates the extent of flow distribution imbalance in each channel of the cold plate at different inlet and outlet positions, as well as the overall flow distribution unevenness. As depicted in **Figure 8(a)**, some channels in the three models with different structures exhibit significantly higher flow distribution imbalance than others. This is because the flow velocity in the channels near the inlet and outlet is higher than the average flow velocity of each channel in the cold plate. In **Figure 8(b)**, the total flow distribution non-uniformity S_t is greatest for the A-type structure (*H*=5mm), followed by B-type (*H*=40mm), and C-type (*H*=80mm). This suggests that relocating the inlet and outlet positions to the middle not only reduces the flow distribution non-uniformity in each channel but also the total flow distribution non-uniformity. In comparison to the A-type model, the flow distribution uniformity in the pump-driven two-phase flow cooling plate with a B-type structure decreases by approximately 57%, while the non-uniformity of flow distribution in the pump-driven two-phase flow cooling plate with a C-type structure decreases by about 72%.

4.2 Impact of sump width on flow distribution uniformity

As observed earlier, relocating the inlet and outlet of the cold plate to the middle enhances the flow distribution in the evaporative cold plate. Building on this observation, the impact of the width of the sump on flow distribution uniformity was analyzed by simulating three different structures with widths of *L*=10, 15, and 20mm.

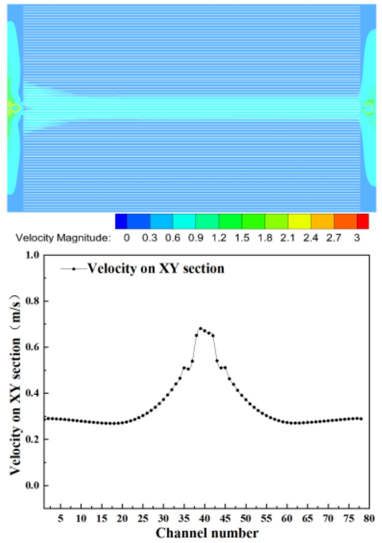

Fig. 9 Velocity contour of the cooling plate and velocity curve of each channel in the XY section when *L*=20mm

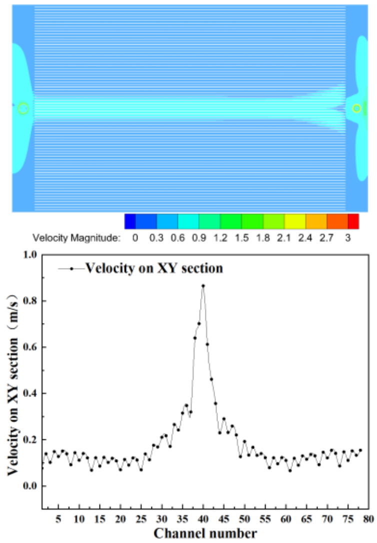

Fig. 10 Velocity contour of the cooling plate and velocity curve of each channel in the XY section when *L*=15mm

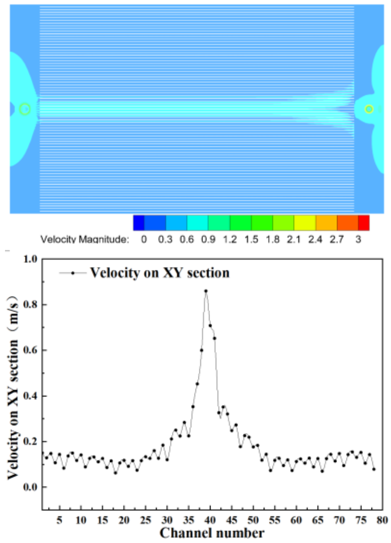

Fig. 11 Velocity contour of the cooling plate and velocity curve of each channel in the XY section when *L*=10mm

Figures 9-11 depict the velocity contour of the cold plate with different sump widths and the velocity curve of each channel in the XY section. The graphs illustrate that, based on the optimal inlet and outlet locations, there are noteworthy peaks in the three velocity charts, all situated near the middle channel. From **Figure 10**, the highest flow velocity in channels 36 to 41 is about 0.9m/s, while the lowest flow velocity in channels 1 to 15 and 65 to 78 is about 0.1m/s, and the highest difference in flow velocity is about 0.8m/s. The flow distribution in the cold plate exhibits significant unevenness. This is attributed to the fact that, upon entering the cold plate through the inlet, the existing eddy current is markedly intensified due to the narrow width of the sump. Influenced by factors such as internal pressure within the cold plate, a substantial amount of fluid is constrained to flow rapidly through the channels located near the inlet and outlet.

Figures 9-11 indicate that the flow distribution in each parallel channel is inadequate when the width of the sump is small. Nevertheless, as the sump width increases to a certain value, the non-uniformity of velocity distribution in the cold plate gradually diminishes. Specifically, with a sump width of L=20 mm, the flow distribution in each channel of the cold plate is relatively uniform. Consequently, it can be inferred that the width of the sump plays a crucial role in ensuring flow distribution uniformity in the pump-driven two-phase flow cold plate.

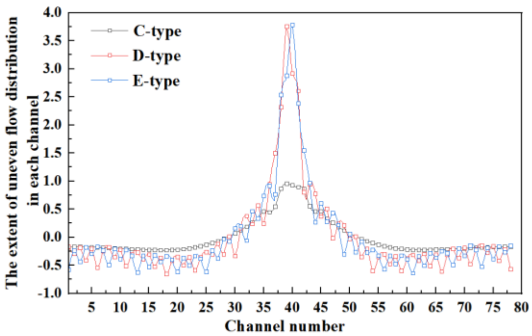

(a) The extent of uneven flow distribution in each channel

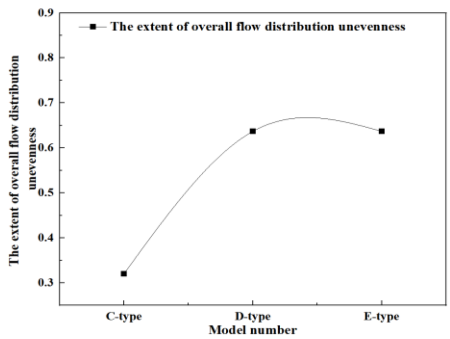

(b) The extent of overall flow distribution unevenness

Fig. 12 Comparative analysis of cold plates with varying sump widths

Figure 12 illustrates the flow distribution imbalance in each channel of the cold plate with varying sump widths, along with the overall flow distribution non-uniformity. **Figure 12(a)** reveals minor disparity in the flow distribution imbalance between the cold plates with D-type and E-type sump widths (L=10mm and L=15mm). The maximum deviation of flow distribution in the cold plate is approximately 3.7, occurring at the inlet and outlet positions, while the minimum deviation is around -0.6, situated in the channels on both sides of the cold plate. For the C-type sump width (L=20mm), the cold plate exhibits a maximum deviation of approximately 1 in flow distribution, situated in the channels at the inlet and outlet positions. The minimum deviation is around -0.1, found in the channels on both sides of the cold plate, indicating the least degree of uneven flow distribution in each channel. In **Figure 12(b)**, when the sump width changes are insignificant, the improvement in the uniformity of the total flow distribution in the cold plate is not apparent. However, as the sump width gradually increases to a certain value, differences in the overall flow distribution unevenness become noticeable in the pump-driven two-phase flow cooling plate. In terms of overall flow distribution unevenness, the flow distribution in the C-type model (L=20mm) is more uniform, approximately 31% lower than that in the evaporative cooling plates with D-type and E-type structures.

4.3 Effect of adding spoiler column at inlet and outlet on flow distribution uniformity

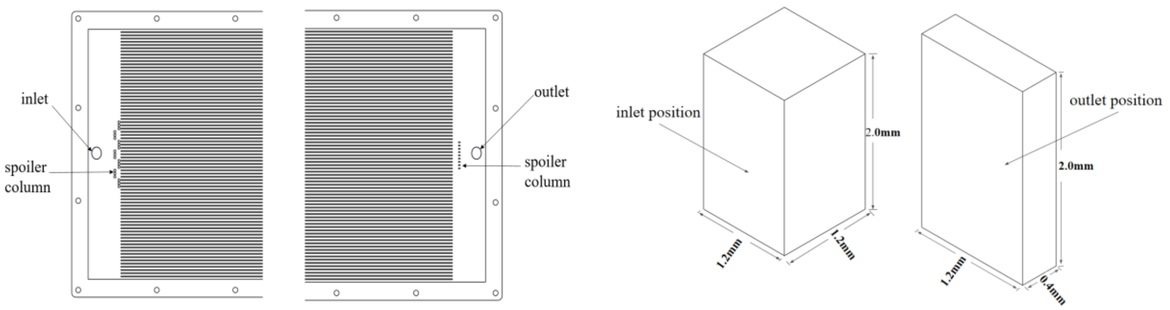

(a) Location of the spoiler column at inlet and outlet (b) Structure of the spoiler column at inlet and outlet

Fig.13 The structure and position of the spoiler column at inlet and outlet

The analysis suggests that flow velocities in channels near the inlet and outlet positions are considerably higher than in other channels. To improve flow distribution uniformity, simulations were conducted on three different structures: one with spoiler columns positioned at the inlet, another with spoiler columns at the outlet, and a third with spoiler columns located at both the inlet and outlet, as depicted in **Figure 13**. This aimed to analyze the impact of adding spoiler columns at the inlet and outlet positions on flow distribution uniformity.

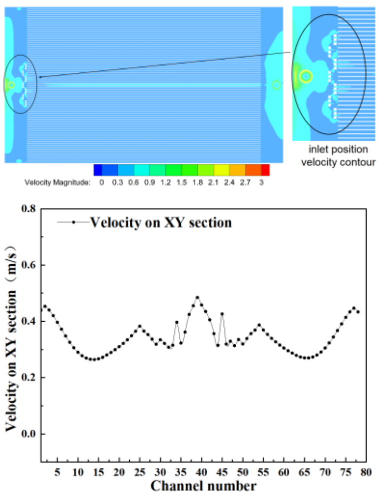

Fig. 14 Velocity contour with spoiler column at the inlet and velocity curve of each channel in the XY section

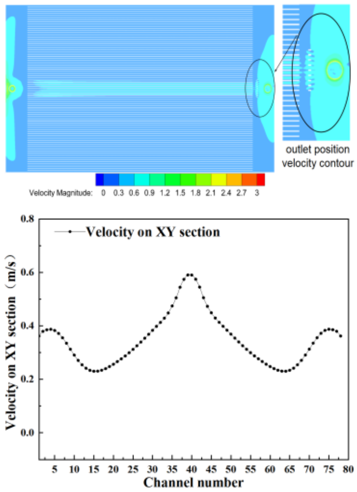

Fig. 15 Velocity contour with spoiler column at the exit and velocity curve of each channel in the XY section

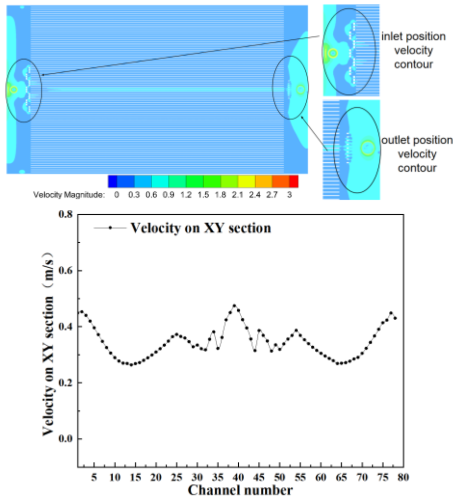

Fig. 16 Velocity contour with spoiler column at inlet and outlet and velocity curve of each channel in the XY section

Figure 14-16 illustrate the velocity distribution under various structural models, along with the velocity curve of each channel in the XY section. These figures clearly show that adding a spoiler column at the optimal inlet and outlet positions, considering the sump width, significantly diminishes the peak values in the three velocity curves. The flow distribution in the cold plate is most uneven when the spoiler column is at the outlet position. The flow distribution is slightly less uniform when the spoiler column is at both the inlet and outlet positions compared to when it's only at the inlet position. Comparing **Figure 7** with **Figure 14** shows that, with fixed inlet and outlet positions and sump width, the flow velocity in each channel is predominantly around 0.32m/s after incorporating the spoiler column at the inlet position. The velocity in the middle and both sides of the channel is slightly higher, reaching approximately 0.45m/s. The fluid forms a vortex in the sump when entering the cold plate through the inlet. However, the spoiler column at the inlet markedly weakens this vortex. As a result, a minor portion of the fluid flows into the middle channels (numbered 38~42), while the majority is distributed to the remaining channels. The channels on both sides receive a higher distribution. The maximum velocity difference within the cold plate channels is merely 0.2 m/s. Consequently, the parallel flow channels in the cold plate with this sump structure exhibit a relatively good distribution uniformity.

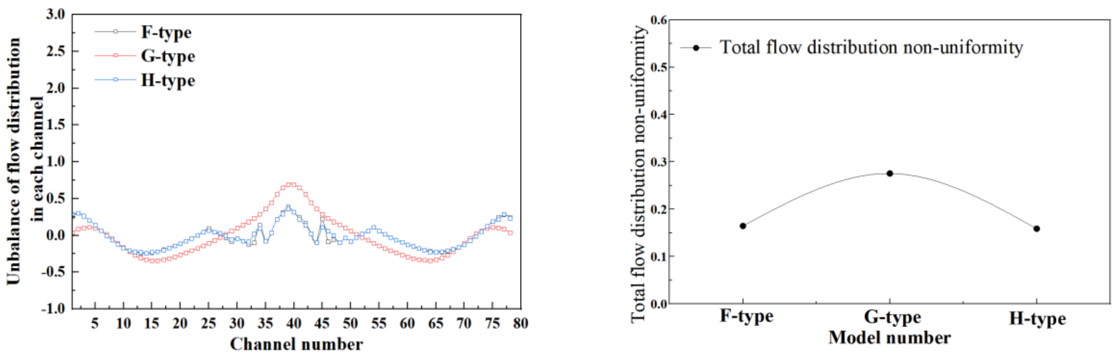

(a) The extent of uneven flow distribution in each channel **(b) The extent of overall flow distribution unevenness**

Fig. 17 Comparison of cold plates with and without spoiler columns at the inlet and outlet

Figure 17 illustrates the flow distribution imbalance in each channel of the cold plate both with and without baffles, as well as the overall non-uniformity in flow distribution. **Figure 17(a)** illustrates a minimal difference in flow distribution imbalance among parallel channels between the F-type and H-type. In the cold plate, the maximum deviation of flow distribution is approximately 0.5, with a minimum deviation of around -0.3. The addition of spoiler columns at the outlet results in a maximum deviation of around 0.7 and a minimum deviation of about -0.4. The results suggest that incorporating spoiler columns at the inlet or at both the inlet and outlet positions enhances the flow distribution balance in each parallel channel of the pump-driven two-phase flow cold plate. **Figure 17(b)** shows that the total flow distribution non-uniformity is highest in the G-type cold plate, followed by the H-type, while the F-type exhibits the smallest non-uniformity. Furthermore, the F-type cold plate, equipped with a spoiler column at the inlet, exhibits a more uniform flow distribution, with a difference approximately 1.5% lower than that of the H-type structure and about 11% lower than the G-type structure.

6. Conclusions

This paper proposes a new flow distribution structure for the evaporative cooling plate in the pump-driven two-phase flow system. The impact of this structure on flow distribution uniformity is investigated through numerical simulations using R134a as the working fluid. This study investigates the impact of inlet and outlet position, sump width, and spoiler column on flow distribution uniformity. The main conclusions can be summarized as follows:

(1) As the inlet and outlet positions deviate from the middle, the overall flow distribution in the channel becomes increasingly uneven. However, placing the inlet and outlet in the middle results in better flow distribution uniformity, reducing non-uniformity by up to 72% compared to having the inlet and outlet on both sides.

(2) With the inlet and outlet positioned in the middle, a narrower sump width results in a more uneven overall flow distribution in the channel, leading to a higher peak flow rate in the middle channel. However, increasing the sump width proves effective in reducing non-uniformity.

(3) The addition of a spoiler column at both the inlet and outlet positions proves effective in reducing flow distribution non-uniformity, achieving a further 17% reduction compared to other structures discussed in this paper. Additionally, incorporating a spoiler column solely at the inlet also yields favorable results.

Declaration of Competing Interest

The authors declare that they have no known competing financial interests or personal relationships that could have appeared to influence the work reported in this paper.

Nomenclature

$\boldsymbol{v}$	—Velocity vector, [m·s^{-1}]	h	—Latent heat of gasification
$\boldsymbol{S}$	—Quality source term, [kg·m^{-3}·s^{-1}]	T	—Temperature, [K]
t	—Time, [s]	m_i	—The fluid flow in the number i channel, [kg·s^{-1}]
$\boldsymbol{a}_h$	—Overload vector, [m·s^{-2}]	m_a	—The average fluid flow in a single channel, [kg·s^{-1}]
$\boldsymbol{F}$	—Volumetric force, [N·m^{-3}]		

		Greek symbols	
E	—Energy, [J]	$\boldsymbol{I}$	—Unit tensor
p	—Pressure, [Pa]	ρ	—Density, [kg·m^{-3}]
Q	—Energy source term, [W·m^{-3}]	α	—volume fraction
r	—Time relaxation coefficient	μ	—Dynamic viscosity, [N·s·m^{-2}]
L	—Width of sump, [m]	λ	—Thermal conductivity coefficient, [W·m^{-1}·K^{-1}]
H	—Distance between inlet and outlet position and upper wall, [m]	ε	—The imbalance of flow distribution
S_t	—Total flow distribution unevenness	κ	—The surface curvature
		σ	—The surface tension, [N·m^{-1}]

Subscripts

l	—Liquid phase	in	—inlet
g	—Gaseous phase	w	—wall

Acknowledgement

The project was supported by Innovation Program of Jiangsu Province (No. SJCX23_1581), Innovation Program of Jiangsu Province (No. SJCX23_1579).

References

[1] Parikh Trupen, Mansour Michael, Thevenin Dominique. Investigations on the effect of tip clearance gap and inducer on the transport of air-water two-phase flow by centrifugal pumps. Chemical Engineering Science, 218 (2020), 115554

[2] Wang J.X, Li Y.Z, Zhang Y, Li J.X, et al. A hybrid cooling system combining self-adaptive single-phase mechanically pumped fluid loop and gravity-immune two-phase spray module. Energy Conversion and Management, 176 (2018), pp. 194-208

[3] Liu X.L, Song B.Y, Zhu Y. Effects of Heat Load and Surrounding Temperature on the Performance of a Pump Driven Two-Phase Thermal Control System. Refrigeration and air conditioning, 31 (2017), pp. 447-452

[4] Tao J.Y. Study on Dynamic Thermal Characteristics of Pumped Two-Phase Flow Loop System, M.D. thesis, Southeast University, Jiangsu, CHN, 2020

[5] Yang G.D, Wang L, Wang J.Y, et al. Research Progress of Refrigerant Uniform Distribution in Microchannel Heat Exchanger. refrigeration. 34 (2015), pp. 33-39

[6] Wu G, Ren T, Ding G. Design and visualized validation of a distributor with uniform refrigerant distribution by forming annular flow. International Journal of Refrigeration, 98 (2018), pp. 238-248

[7] Setyawan, Iwan, Putra, Nandy, Hakim, Imansyah Ianu. Experimental investigation of the operating characteristics of a hybrid loop heat pipe using pump assistance. Applied thermal engineering: Design, processes, equipment, economics, 130 (2018), pp. 10-16

[8] Jiang C, Liu W, et al. Experimental investigation of pump-assisted capillary phase change loop. Applied thermal engineering: Design, processes, equipment, economics, 71 (2014), pp. 581-588

[9] Wang Z.R, Zhang X.B, Wen S.Z, et al. Design and performance of a mechanically pumped two-phase loop to support the evaporation-condensation experiments on the TZ1. Case Studies in Thermal Engineering. 10 (2017), pp. 650-655

[10] Wu X, Gao Z, Meng H, et al. Experimental study on the uniform distribution of gas-liquid two-phase flow in a variable-aperture deflector in a parallel flow heat exchanger. International Journal of Heat and Mass Transfer, 150 (2020), 11935

[11] Peng X, Li D, Li J, et al. Improvement of Flow Distribution by New Inlet Header Configuration with Splitter Plates for Plate-Fin Heat Exchanger. Energies, 13 (2020), pp. 13-23

[12] Byun HW, Kim NH. Two-phase refrigerant distribution in an intermediate header of a parallel flow minichannel heat exchanger. International Journal of Refrigeration, 59 (2015), pp. 14-28

[13] Yuan P, Hong C, Dan L. The flow distribution uniformity research on the microchannel parallel flow heat exchanger. Cryogenics and Superconductivity, 47 (2019), pp. 44-48

[14] Wei M, Fan Y.L, Luo L.A, et al. CFD-based evolutionary algorithm for the realization of target fluid flow distribution among parallel channels. Chemical Engineering Research & Design, 100 (2015), pp. 341-352

[15] Gao Z.C, Meng H, Wang Y.L. Study on distribution characteristics of aperture-changeable deflector in parallel flow heat exchanger. Cryogenics and Superconductivity, 46 (2018), pp. 63-68

[16] Tian Y.S, Jiao Y.G, Sun H.K, et al. Structural Optimization and Flow Characteristics of the Interrupted Microchannels. Journal of Mechanical Engineering,59(2023), pp. 274-282

[17] Redo M. A, Jeong J, Yamaguchi S, et al. Characterization and improvement of flow distribution in a vertical dual-compartment header of a microchannel heat exchanger. International Journal of Refrigeration, 116 (2020), pp. 36-48

[18] Siddique A, Medhi B. J, Agrqwal A, et al. Design of a collector shape for uniform flow distribution in microchannels. Journal of Micromechanics and Microengineering, 27(2017), 075026

[19] Wu G. M, Yan Z. T, Zhuang D. W, et al. Design method and application effects of embedded-clapboard distributor on refrigerant distribution among multi-tubes of micro-channel heat exchangers. International Journal of Refrigeration, 119 (2020), pp. 420-433

[20] Ye A. Q, Wang J. J, Zhong H, et al. Refrigerant Distribution Performance of Dry-expansion Evaporator. Journal of Chemical Engineering, 43 (2022), pp. 73-80

[21] Zhao L. P, Wang R. J, Liu G. L, et al. Characteristics of refrigerant flow distribution in parallel flow evaporator, Journal of Tongji University (Natural Science), 47 (2019), pp. 261-268

[22] Han Q, Zhang C, Chen J. P. Experimental and CFD investigation of R410A distributors for air conditioner, International Journal of Air-Conditioning and Refrigeration, 22 (2014), 1440002

[23] Brackbill J. U, Kothe, D. B, Zemach C. A continuum method for modeling surface tension. Journal of Computational Physics, 100 (1992), pp. 335–354

[24] Lee W. H. A Pressure Iteration Scheme for Two-Phase Modeling. Los Alamos, New Mexico, Los Alamos Scientific Laboratory, 1979

[25] Habib M. A, Ben-Mansour R, Said S, et al. Evaluation of flow maldistribution in air-cooled heat exchangers, Computers & Fluids, 38 (2009), pp. 677-690

Submitted: 14.12.2023.

Revised: 03.04.2024.

Accepted: 15.04.2024